BMC Pediatrics

RESEARCH

Open Access

Hand X-rays findings and a disease screening for Turner syndrome through deep learning model

Yirou Wang[1†], Yumo Wang[2†], Feihan Hu[1], Liqi Zhou[3], Yu Ding[1], Chen Guo[4], Yao Chen[1], Yabin Hu[5], Shijian Liu[5] and Xiumin Wang[1*]

Abstract

Background Turner syndrome (TS) is one of the important causes of short stature in girls, but there are cases of misdiagnosis and missed diagnosis in clinical practice. Our aim is to analyze the hand skeletal characteristics of TS patients and establish a disease screening model using deep learning.

Methods A total of 101 pediatric patients with TS were included in this retrospective case-control study. Their radiation parameters from hand X-rays were summarized and compared. Receiver operating characteristic (ROC) curves for parameters with differences between the groups were plotted. Additionally, we used deep learning networks to establish a predictive model.

Results Four parameters were identified as having diagnostic value for TS: the length ratio of metacarpal IV and metacarpal III, the distance between ulnoradial tangents, the carpal angle, and the ulnar-radial angle. When the cutoff value of the distance between the ulnoradial tangents was 0.40 cm, the specificity reached 92.57%. And for the ulnar-radius angle, according to the ROC analysis, the maximum value of Youden's index was obtained when the cut-off value was 170°, with a sensitivity of 66.34% and specificity of 61.38%. The ResNet50 deep neural network architecture was utilized, resulting in an accuracy of 78.89%, specificity of 76.67%, and sensitivity of 83.33% on a test dataset.

Conclusions We propose that certain hand radiograph parameters have the potential to serve as diagnostic indicators for TS. The utilization of deep learning models has significantly enhanced the precision of disease diagnosis.

Keywords Turner syndrome, Hand X-rays, Deep learning, Disease screening, Short stature

[†]Yirou Wang and Yumo Wang contributed equally to this work.

*Correspondence:
Xiumin Wang
wangxiumin@scmc.com.cn
[1]Department of Endocrinology, Genetics and Metabolism, Shanghai Children's Medical Center, School of Medicine, Shanghai Jiao Tong University, Shanghai, China
[2]School of Intelligent Manufacturing, Nanjing University of Science and Technology, Nanjing, China
[3]Department of Data Science, School of Statistics and Information, Shanghai University of International Business and Economics, Shanghai, China
[4]Diagnostic Imaging Center, Shanghai Children's Medical Center, School of Medicine, Shanghai Jiao Tong University, Shanghai, China
[5]Department of Clinical Epidemiology and Biostatistics, Shanghai Children's Medical Center, School of Medicine, Shanghai Jiao Tong University, Shanghai, China

Introduction

Turner syndrome (TS) is a relatively common chromosomal disorder in which female patients typically have short stature and hypogonadism owing to the absence of the X chromosome [1, 2]. TS occurs in 1/2000 of live female birth [3]. However, in reality, this condition may remain undiagnosed or diagnosed later. One of the reasons for this situation is the lack of simple and effective screening methods that can identify TS from normal girls.

In the previous studies, the median age at diagnosis varied from 1.5 to 15.1 years [3, 4]. Many patients are not diagnosed until they present with primary amenorrhea or infertility [3]. Sarah et al. found that in their cohort, the median age at diagnosis was 9.3 years if there was no diagnosis 1 year after birth [4]. A study from the UK Biobank in 2018 reported that many women with TS were not diagnosed until they were adults and some were never diagnosed [5].

Early diagnosis and treatment are of great significance for patients with TS. Growth hormone treatment can bring them close to normal female final height, and sex hormone therapy helps maintain secondary sex characteristics, uterine development, bone density, and mental health [6].

Karyotype analysis is the gold standard for diagnosing Turner syndrome. However, owing to its technical requirements and cost-effectiveness, it has not yet been used in large-scale clinical screening programs. Clinically, testing is mostly considered in patients with typical TS symptoms. However, the accuracy of patient clinical evaluation is largely dependent on the personal knowledge and experience [7]. Common clinical manifestations of TS include growth failure (95–100%), infections of the middle ear (60%) and mandible (60%), and nonverbal learning disabilities (~40%), all of which are not disease-specific [1]. There was significant variation between individuals, and variation in karyotypes may be associated with the phenotype. In general, women with monosomy 45,X were more affected than those with other karyotypes. However, compared to patients with other karyotypes, patients with 45, X had a slightly lower median age at diagnosis [8]. In cases with mild clinical manifestations, short stature can be the sole evident manifestation in childhood. Meanwhile, because the test report usually takes approximately 4–5 weeks, it may lead to patient loss to follow-up. Therefore, we aimed to use the information provided by routine tests to develop a rapid and low-cost TS screening method.

As mentioned above, patients with TS often visit the hospital for short stature in childhood, and hand radiography is the most routine examination for children with short stature [4]. The hand bones consist of both irregular and long bones, and as children grow older, multiple ossification centers gradually appear. Hand X-rays are often used to assess bone age or maturity to determine growth potential, and skeletal abnormalities can be detected. Skeletal deformities are a clinical manifestation of Turner syndrome in which various hand deformities have been observed. These include short fourth and fifth metacarpals, positive metacarpal signs, Madelung deformity, and a narrow carpal angle (Fig. 1) [9]. However, very few studies have analyzed the characteristics of radiological hand parameters in patients with TS or evaluated the early diagnostic value of these parameters in TS. Therefore, we chose to develop a screening model

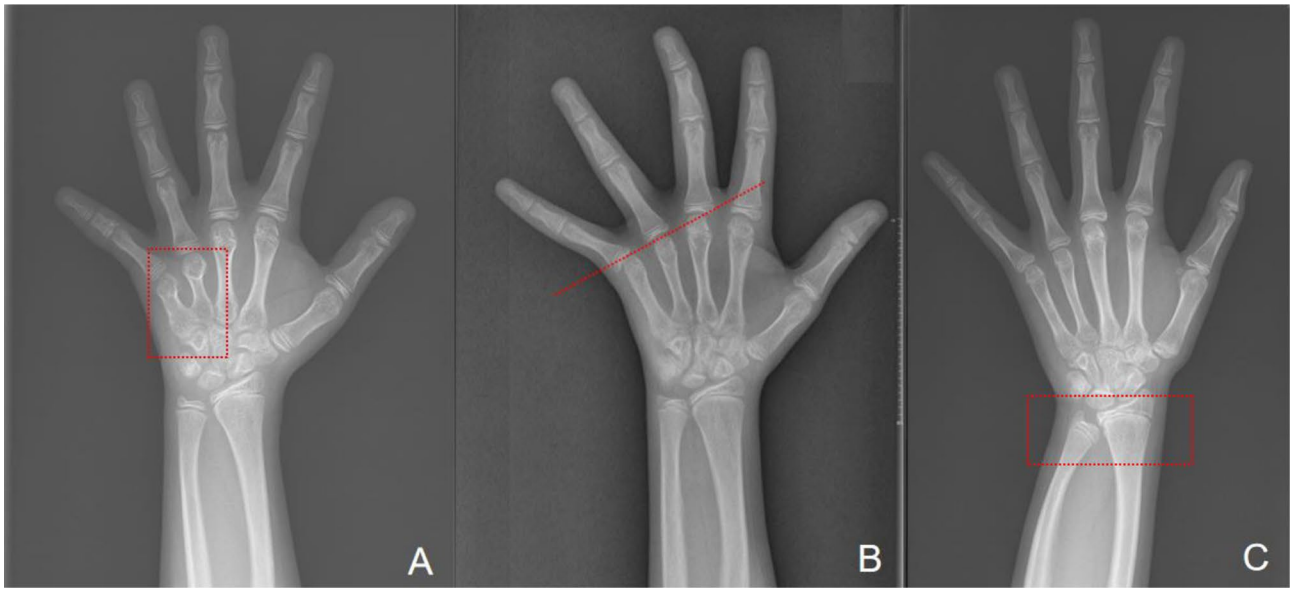

Fig. 1 Skeletal deformities of TS patients. **A**. short fourth and fifth metacarpals. **B**. positive metacarpal sign. **C**. Madelung's deformity

using hand X-ray images, which was a necessary and simple examination method for TS, and TS has characteristic feature in hand bones that could provide an abundance of information.

In this study, we measured and analyzed radiological hand parameters in 101 patients with TS and compared them with those of a control group of 202 girls with short stature and normal karyotypes. Combined with the differential parameters of the case and control groups, we evaluated their diagnostic value in TS. Furthermore, we attempted to use an image-recognition model based on deep learning to determine the role of hand X-ray images in TS screening and recognition, which may have important significance for the early diagnosis of this disease.

Subjects and methods

Study participants

This study was conducted at Shanghai Children's Medical Center, Shanghai Jiao Tong University School of Medicine, Shanghai, China(Filing number: MR-31-24-010836, https://www.medicalresearch.org.cn). The participants were girls admitted to the hospital for short stature from January 1, 2019, to December 31, 2022, each of whom had completed chromosome karyotype testing. Based on the clinical manifestations and karyotypes, we identified 101 patients diagnosed with TS. Here, considering the difference in the ossification center at different ages and the difference in bone size at different heights, we conducted a case-control study in which we randomly 1:2 matched age-and height-specific controls in girls with normal karyotypes ($n = 202$). In the control group, we excluded children with intellectual disabilities, short stature syndrome caused by single gene mutations, and congenital malformations in other systems. All participants, due to their short stature, underwent complete chromosome karyotype analysis during clinical diagnosis and treatment. Informed consent was obtained from the children and their parents. The study was approved by the Institutional Review Board of the Shanghai Children's Medical Center (No. SCMCIRB-YSWJW2023008).

Hand X-ray feature evaluation

In this study, hand X-ray images were used to evaluate the hand bone morphology. All X-rays were taken on the left hand with the five fingers naturally separated and the thumb and palm at a 30° angle. The axis of the middle finger was aligned with the axis of the forearm, and the source-image distance was constant (80 cm). To quantify hand abnormalities, several radiological hand parameters were measured independently by two physicians in the Department of Radiology with more than 5 years of experience. The average values of the two observers for each parameter were calculated for further analysis. Based on the hand bone characteristics of TS, we focused on the length of the metacarpals and changes in carpal space, which include measurements of angles and heights. The following parameters were calculated and observed (Fig. 2).

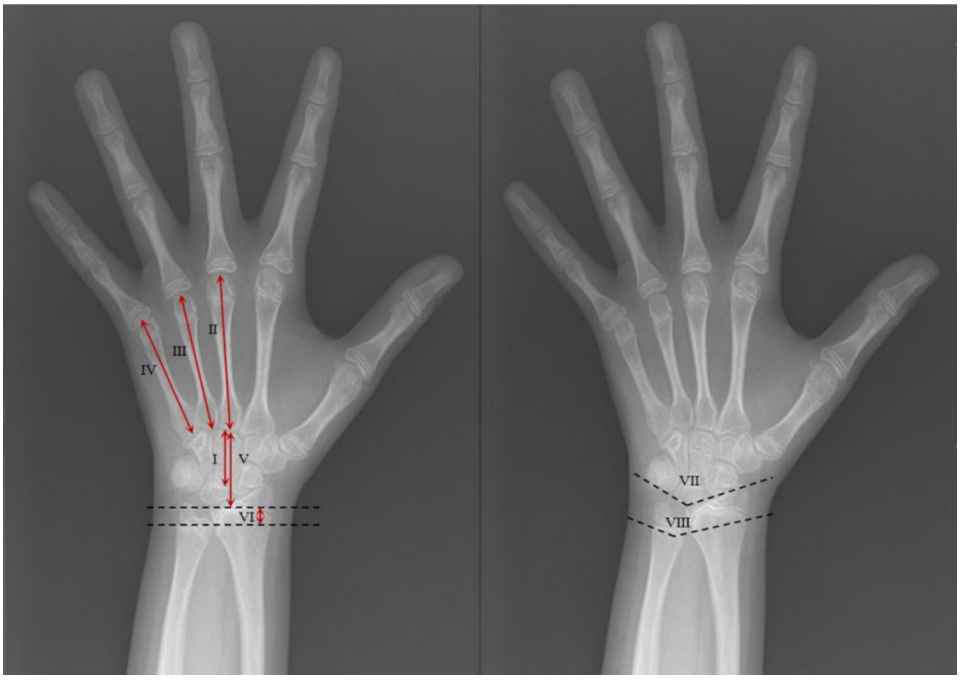

Fig. 2 Demonstration of measurements performed on Hand X-ray of a patient. Parameters include: Capitate bone length (I), Metacarpal III length (II), Metacarpal IV length (III), Metacarpal V length (IV); Carpal height (V, the distance from the apex of Capitate to the Radius dome); The distance between ulnoradial tangents (VI); Carpal angle (VII), Ulnar-Radial angle (VIII)

1. Bone length: capitate bone, third metacarpal bone (metacarpal III), fourth metacarpal bone (metacarpal IV), and fifth metacarpal bone (metacarpal V).
2. Angle: Carpal angle (VII) (the angle between the tangents of the scaphoid lunate bone and lunate-deltoid bone) and ulnar-radial angle (VIII) (the angle between the distal radius and ulna);
3. Distance: the distance between ulnoradial tangent (VI);
4. Carpal height (V): distance between the base of the third metacarpal and the subchondral bony cortex of the distal radius.
5. Carpal height ratio: value of dividing carpal height by the length of the third metacarpal [10].
6. Nattrass index: the value of dividing carpal height by the length of capitate bone [11].
7. Positive metacarpal sign: If the line drawn along the heads of the 4th and 5th metacarpals intersects with the head of the 3rd metacarpal bone, it is considered positive [12].

Deep learning technique

We implemented medical diagnostic classification of X-ray images using the ResNet50 network [13]. Next, we provide a detailed description of our methodology (Fig. 3).

Data set and data pre-processing

We selected a dataset consisting of 202 nondiseased and 101 diseased X-ray images for the deep learning network. To ensure the generalizability of the model, we randomly split the dataset into 55% for training, 15% for validation, and 30% for testing. The input image size for ResNet50 was $224 \times 224 \times 3$, whereas the acquired X-ray images had nonuniform sizes. Thus, we employed image resizing and normalization techniques to conform to the input requirements of a deep learning network. Owing to the limited data quantity and variations in hand positioning in X-ray images, we also applied data augmentation techniques, such as random horizontal and vertical flipping, random rotation, and random zooming, to increase the size of the training set and reduce overfitting. The selection of these specific augmentation techniques was

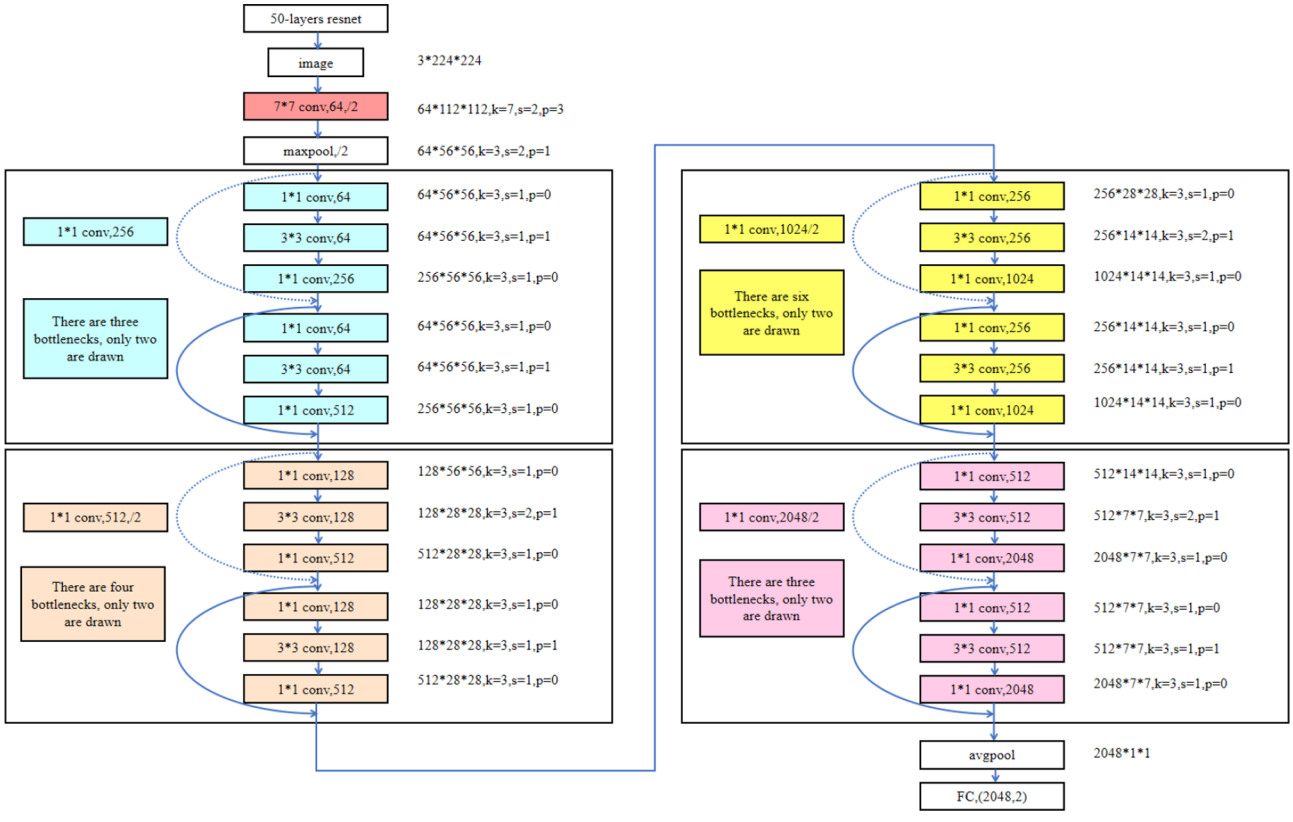

Fig. 3 The deep learning network structure based on a modified version of ResNet50. The network input size is 3*224*224, where 3 represents the number of channels and 224*224 represents the image size. The convolution calculation for each layer is shown in the diagram to the right of each convolution kernel, such as "64*112*112, k = 7, s = 2, p = 3", where 64 represents the number of feature channels, 112*112 represents the feature size, k represents the convolution kernel size, s represents the convolution stride, and p represents the padding around the feature. The symbol "/2" in the diagram represents downsampling, which reduces the output feature size by half. There are a total of 50 layers in ResNet50, with the same bottlenecks shown schematically in the diagram

based on their commonality and effectiveness in image data augmentation. For instance, data flipping simulated the effects of mirror reflection, while data rotation simulated different shooting perspectives. Changes in brightness simulated images under various lighting conditions, which was particularly important for improving the model's performance in different environments.

Network

We used the ResNet50 deep neural network architecture, which has shown excellent performance in various computer-vision tasks. We replaced the last fully connected layer of ResNet50 with a new layer with two output neurons corresponding to the two disease classes.

Training

We trained the ResNet50 model on the training set using the stochastic gradient descent optimizer with a learning rate of 0.00001, batch size of 32, and categorical cross-entropy loss function. We trained the model for 100 epochs and saved the model weights with the best performance on the validation set.

Evaluation

We evaluated the trained model using the test set and calculated the accuracy, precision, recall, and F-score for each disease class. We also generated a confusion matrix and calculated the area under the receiver operating characteristic curve for each disease class.

Statistical analysis

For descriptive analyses, continuous variables are summarized as mean ± standard deviation (SD) or median (interquartile range, IQR), and categorical variables are presented as frequencies and percentages. Comparisons of basic characteristics among groups were analyzed using the Mann-Whitney U test for skewed continuous variables, Student's t-test for normally distributed continuous variables, and the Pearson Chi-square test for categorical variables. Receiver operating characteristic (ROC) curves for the parameters were plotted and the area under the curve (AUC) was measured. In addition, we used deep learning networks to analyze the images and attempt to establish predictive models. All statistical analyses were performed using SPSS 25.0 (SPSS Inc., Chicago, IL, USA) and the ResNet50 network, and statistical significance was set at two-tailed $p < 0.05$. And in our study, to ensure matching between the control group and the experimental group in terms of age and height, we used SPSS software to carry out the matching process. The matching functionality of SPSS software allowed us to make precise pairings based on the statistical distribution of these variables, ensuring comparability between the two groups.

Results

Karyotypes distribution

A total of 101 girls were enrolled in the TS group, including those with monosomy X (45, X, $n = 52$), mosaicism (45, X/46, XX, $n = 12$; mosaicism with triple X, $n = 3$; mosaicism with Y chromosome, $n = 1$), deletion (partial deletion of one X chromosome, $n = 23$), and X isochromosome ($n = 10$) (Fig. 4). The karyotypes of all girls in the control group were 46, XX. There were no significant differences in age or height between the two groups (Table 1).

Characteristics of hand X-ray parameters

According to the measurement and statistics of the radiological hand parameters, the length ratio of metacarpals IV and III, carpal angle, and ulnar-radial angle in the TS group were lower than those in the control group (0.86 vs. 0.88°, $p = 0.002$; 125.27°vs. 129.26°, $p = 0.002$; and 167.76°vs. 173.08°, $p < 0.001$, respectively) (Table 1). The distance between the ulnoradial tangents was greater in the TS group than in the control group (0.25 vs. 0.00, $p < 0.001$) (Table 1).

Based on the ROC analysis, we found that the AUC length ratio of metacarpal IV and metacarpal III (Fig. 5A, AUC = 0.638), distance between the ulnoradial tangents (Fig. 5B, AUC = 0.661), carpal angle (Fig. 5C, AUC = 0.626), and ulnar radial angle (Fig. 5D, AUC = 0.699) had diagnostic value for TS. Furthermore, we determined the sensitivity and specificity of the four parameters for different cutoff values (Table 2).

Sensitivity and specificity of single hand X-ray parameters

The appropriate cutoff value of the ulnar-radial angle (VIII) was 170 °when Youden's index reached a maximum value of 0.277, and the sensitivity and specificity were 66.34% and 61.38%, respectively (Table 2). This suggests that the possibility of Turner syndrome should be further considered when the ulnar radial angle is less than 170 °on the radiogram of a girl with short stature. As a screening indicator, the cut-off value of the carpal angle was 130 °, and high sensitivity and specificity were obtained, with 73.42% and 41.67%, respectively.

Analysis of deep learning models

The network performance was tested on 30% (90 303) of the images that were not used for training. The metrics used were accuracy (proportion of successful classifications), sensitivity (recall, proportion of positively labeled images that were classified correctly), and specificity (proportion of correctly classified negative images). The ensemble model, which was averaged over the output of multiple networks, showed a confusion matrix result with an accuracy of 78.89%, specificity of 76.67%, and sensitivity of 83.33% on the test images (Fig. 6A). The ROC curve

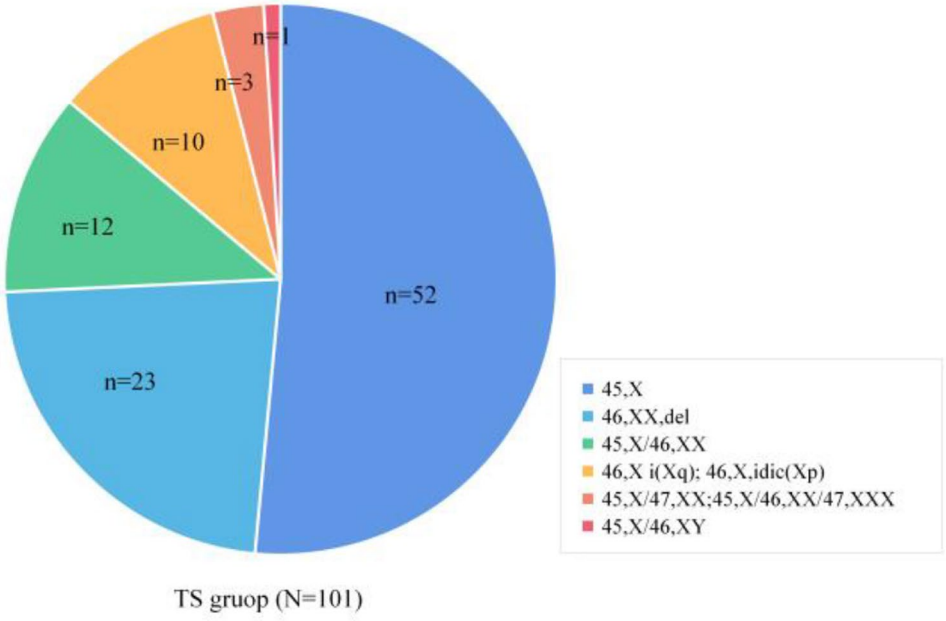

Fig. 4 Type and frequency of chromosome abnormalities in TS group

is shown in Fig. 6B, showing the relationship between the false positive rate and the true positive rate for different classification threshold values; the AUC was 0.865. Figure 6C presents the precision-recall curve, which shows a similar tradeoff between precision (proportion of positively classified images that were correctly classified) and recall, with an AUC of 0.794. Both figures show the broad range of thresholds for which both high-performance metrics are attainable. In addition, the binary decision of whether a patient has TS is based on an activation score between 0 and 1 output by the network, corresponding to the probability that the network assigns to the positive label. We generated a histogram of these scores (Fig. 6D) and observed that the most correctly classified points accumulated at the edges, whereas the incorrectly classified images were more spread out along the X-axis.

Discussion

In this study, we summarized the hand skeletal characteristics of TS by measuring and analyzing radiological parameters from hand radiographs. Through case-control studies, we found that certain characteristic parameters can be used as indicators for TS screening in girls with short stature. Therefore, we developed an algorithm for automatic TS screening based on artificial intelligence and deep learning that mainly focuses on hand X-ray image features.

Previous studies have described radiological abnormalities of the hand in Turner syndrome and discussed the diagnostic value of this disease [2, 10, 14]. To ensure there were no differences in age and height between the two groups, we conducted a case-control study that ensured that the X-ray images between the two groups were not affected by these factors. Our study evaluated hand X-ray features based on the bone length, length ratio, angle, and tangential distance. For bone length, shortness of metacarpals IV and V is one of the features of TS that can be reflected by the metacarpal sign [15]. On a normal radiograph of the hand, a line was drawn at the tip of metacarpal IV and metacarpal V. The distal end of this line was beyond the tip of the third metacarpal bone and the metacarpal sign was negative. This sign is positive in some patients with TS due to the short metacarpal bone. Park et al. found that the positive rate of metacarpal signs in the TS group was 33.8%, based on the analysis of hand radiographs of 81 patients with TS [12]. In the present study, this proportion was 21.78% and 8.41% in the TS and control groups, respectively. However, in some cases, when patients with TS have only a short metacarpal V, the metacarpal sign can also be negative. Therefore, it is not appropriate to use only the metacarpal sign to evaluate metacarpal shortness in patients with TS [15]. Therefore, in this study, we measured the lengths of metacarpals III, IV, and V in all individuals in the TS and control groups and calculated the length ratio of metacarpals IV and III and the length ratio of metacarpals V and III. Surprisingly, there were no statistically significant differences in the lengths of metacarpals III, IV, and V between the two height-matched groups. The length ratio of metacarpal IV to metacarpal III was lower in the TS group than that in the control group (0.86 vs. 0.88, $p = 0.002$). This result indicated that shortening

Table 1 Hand X-ray features evaluation in TS patients and matched controls

Characteristics	TS ($n=101$)	Controls ($n=202$)	Statistics T/Z/χ^2	*p*-value
Age (months)	103.31 ± 30.89	102.54 ± 32.34	-0.196	0.841
Height (SD)	-2.16(0.19)	-2.18(0.16)	-0.204	0.838
Length(cm)				
Carpal bone	1.71 ± 0.33	1.64 ± 0.34	-1.340	0.181
Metacarpal III	4.11 ± 0.73	4.09 ± 0.83	-0.143	0.887
Metacarpal IV	3.51 ± 0.65	3.57 ± 0.76	0.648	0.518
Metacarpal V	3.29 ± 0.59	3.28 ± 0.71	-0.184	0.854
Carpal height	2.51 ± 0.28	2.48 ± 0.30	0.419	0.419
Length ratio				
Metacarpal IV/ Metacarpal III	0.86(0.04)	0.88(0.04)	-4.080	**0.002**
Metacarpal V/ Metacarpal III	0.80(0.05)	0.80(0.05)	-0.760	0.439
Distance (cm)				
Between ulnoradial tangents	0.25(0.39)	0.00(0.23)	4.797	**< 0.001**
Angles (°)				
Carpal angle	125.27 ± 9.66	129.26 ± 8.76	-3.151	**0.002**
Ulnar-Radial angle	167.76 ± 6.89	173.08 ± 7.13	6.201	**< 0.001**
Carpal height ratio	0.61 ± 0.09	0.62 ± 0.11	0.459	0.459
Nattrass index	1.45 ± 0.22	1.46 ± 0.22	0.513	0.608
Positive metacarpal sign	17/202(8.41%)	22/101(21.78%)	10.727	**0.001**

Bold indicates $p < 0.05$

Mann-Whitney tests were used for skewed continuous variables

T tests were used for normally distributed continuous variables

χ^2 tests were used for categorical variable

of metacarpal IV relative to metacarpal V is frequently observed in patients with TS.

The carpal and ulnar radial angles were also measured. It has previously been reported that patients with TS have relatively narrow carpal angles [16]. Necić et al. evaluated radiographs of the left hand in 17 patients with TS and 17 age-matched girls with constitutional short stature and found no statistical difference in the carpal angle between the two groups. The mean values for both groups were almost identical (TS: 124.7° vs. control: 125.1°) [2], but in the present study, the mean value of the carpal angle in the TS group was significantly lower than that in the control group, with a statistical difference (TS 125.27°±9.66° vs. control 129.26°±8.76°, $p=0.002$). When the carpal angle cut-off point was 120°, although the sensitivity decreased to 34.18%, the specificity was 84.62%. This suggests that when reading the wrist radiographs of girls with short stature, TS should be further considered if the carpal angle is < 120 °. Madelung deformity is a specific skeletal abnormality associated with TS [17]. The main change in this deformity is the short and curved radius, with the wrist facing the volar and ulnar sides slanting. To quantify this change, we measured the ulnar-radial angle (Fig. 1) and the distance between ulnoradial tangents (Fig. 1). When the ulna and radius were in the same horizontal plane, the ulnar-radial angle was 180° and the distance between the tangents was 0 cm. In our study, the mean value of the ulnar-radial angle in the TS group was only 167.76°, and the median distance between ulnoradial tangents reached 0.25 cm, both of which were statistically different from those in the control group. Tauber et al. found that the greater the value of this parameter, the greater the height gain after growth hormone treatment, which was not evaluated in our study [14]. Our study showed that when the cutoff value of the distance between the ulnoradial tangents was 0.40 cm, the specificity reached 92.57%, suggesting that this sign is clinically significant in diagnosing TS. For the ulnar- radius angle, according to the ROC analysis, the maximum value of Youden's index was obtained when the cut-off value was 170°, with a sensitivity of 66.34% and specificity of 61.38%. These findings suggested that clinicians should have considered the diagnosis of Turner syndrome and conducted relevant assessments when they encountered short girls with a distance between the ulnar-radial tangents exceeding 0.40 cm or an ulnar-radius angle less than 170°.These measurements can be completed in an outpatient clinic, potentially reducing the missed diagnosis rate of TS.

In recent years, with the widespread application of artificial intelligence technology in the field of biomedicine [18, 19]. Because the screening index of TS cannot achieve good results using any of the above parameters alone, we attempted to establish a better screening model using artificial intelligence image recognition, which achieves the comprehensive efficiency of the joint prediction of multiple parameters. We developed a deep learning model to classify hand X-ray images as patients with TS or controls, achieving an accuracy of 78.89%, specificity of 76.67%, and sensitivity of 83.33% on a test dataset. In this dataset, the model made five false-negative and 14 false-positive judgments. We analyzed the reasons for these errors from the perspective of age and karyotype. From the perspective of age, false positives appeared at all ages, but the error rate was the highest in the younger age group (less than 60 months). The judgment of three-fifths of the patients was false positives, which indicated that the occurrence of false positives might be related to the fewer ossification centers at the young age group, so there were fewer identifiable features in the image (Fig. 7A). In the TS group of the test dataset, the judgments of five of the 30 patients were false negatives. By analyzing the distribution of chromosome karyotypes, we found that patients with haplotypes 45, X were all identified by our

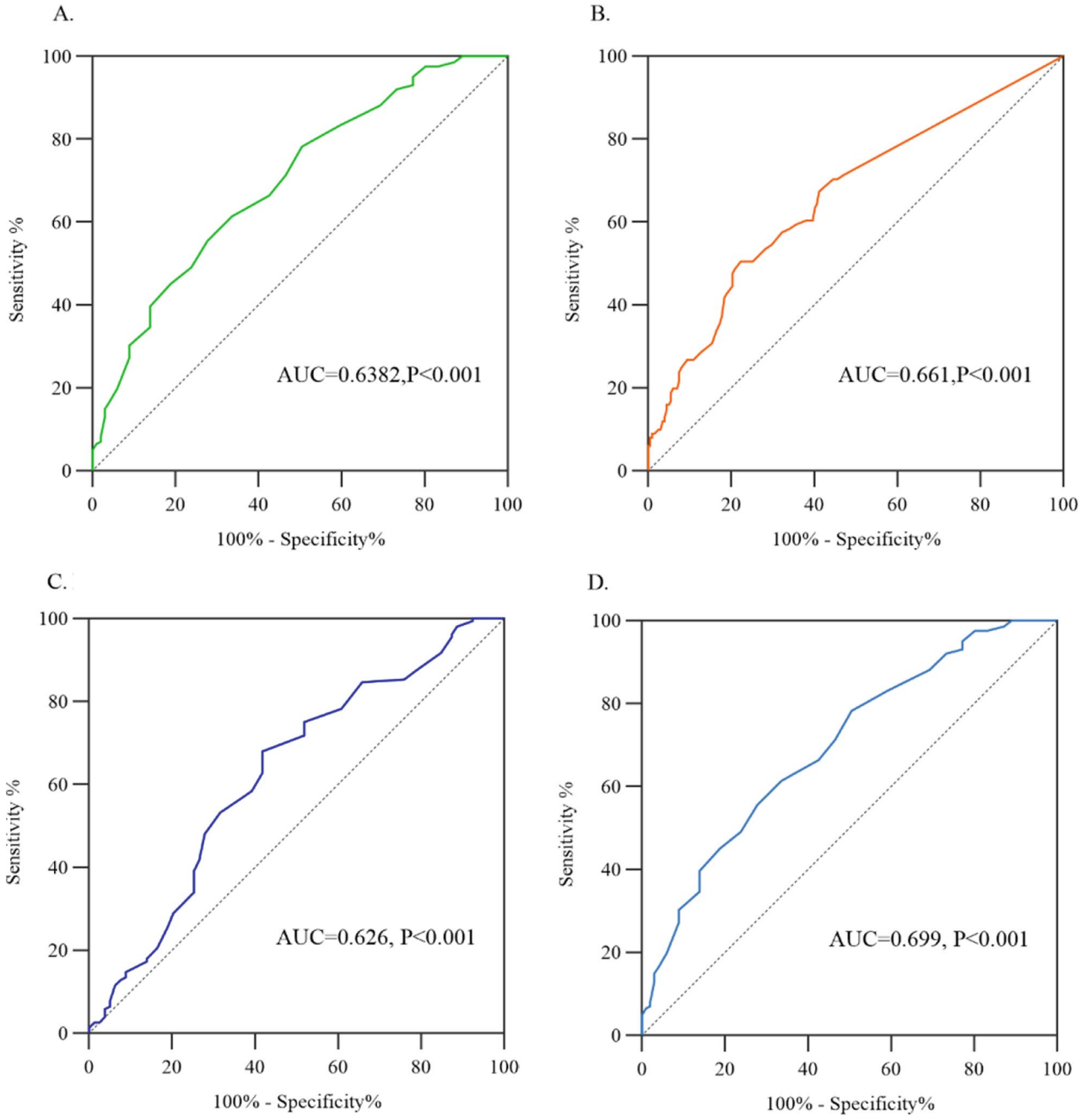

Fig. 5 **A**. ROC curves of the four parameters predictors of TS. ROC curve of length ratio of metacarpal IV and metacarpal III. **B**. ROC curve of the distance between ulnoradial tangents. **C**. ROC curve of the carpal angle. **D**. ROC curve of the ulnar-radial angle

model, while all five cases with incorrect judgments were other karyotypes (three were 45, X/46, XX, one was 46, XX, del (p.22.2), and one was 45, X/47, XXX) (Fig. 7B). This indicates that haploid TS not only has more severe clinical symptoms but also has more obvious features on hand bone images. Our model efficiently and accurately identifies patients with TS and haploid karyotypes. The clinical scenario for this model was as follows: after a short girl has her hand X-ray image taken, once the image is uploaded to the model, the model will output a classification result, which will indicate to the clinician whether chromosomal karyotyping is necessary.

In recent years, the use of machine learning and deep learning methods for the diagnosis and research of TS has gained increasing attention. Existing studies have primarily employed entire facial images as datasets [20–22]. Screening through facial images appeared to achieve similar sensitivity and specificity as our study. However,

Table 2 Sensitivity and specificity of different hand X-ray skeletal measurement parameters for predicting Turner syndrome

Parameters	Cutoff	Sensitivity,%	Specificity, %	Youden's index	PPV, %	NPV, %
Length ratio of metacarpal IV and metacarpal III	0.88	79.21	35.64	0.148	38.10	77.42
	0.86	56.43	67.32	0.237	46.34	75.56
	0.84	29.70	86.13	0.158	51.72	71.02
Distance between ulnoradial tangents (VI) (cm)	0.10	70.29	54.45	0.247	43.56	78.57
	0.20	54.45	70.29	0.247	47.82	75.53
	0.30	37.62	82.18	0.198	51.35	72.49
	0.40	21.78	92.57	0.144	59.45	70.30
Carpal angle (VII) (°)	130	73.42	41.67	0.151	38.93	75.59
	125	58.23	62.82	0.211	44.23	74.81
	120	34.18	84.62	0.188	52.94	71.73
Ulnar-radial angle (VIII) (°)	175	86.13	34.65	0.208	39.73	83.33
	170	66.34	61.38	0.277	46.21	78.48
	165	30.69	88.11	0.188	56.36	71.78
	160	16.83	97.52	0.144	77.27	70.10

PPV, positive predictive value; NPV, negative predictive value

from a clinical application perspective, obtaining hand X-rays was more routine and did not involve patient privacy. From the perspective of classification techniques and methodologies, we chosen Convolutional Neural Networks (CNNs), which strike a better balance between performance and computational efficiency. CNN had been widely applied and validated across various domains and tasks, including medical image analysis [23]. In the research on TS, Liu et al. utilized Convolutional Recurrent Neural Networks (CRNN) in deep learning, focusing on learning facial image features of TS patients and combining them with Support Vector Machines (SVM) for the classification of TS [21]. Li et al. adopted methods such as Support Vector Machines (SVM) and Principal Component Analysis (PCA) to extract and analyze facial image features, assisting doctors in the clinical assessment of TS patients [22]. we will also compare the performance merits and demerits of different deep learning models in the future.

We will test this model in a clinical setting, expand the dataset, and optimize its performance. We plan to use this model to classify karyotypes of patients with TS. In summary, we believe that this model can provide clinicians with risk tips for Turner's during outpatient visits for girls with short stature to achieve early diagnosis.

Study strengths and limitations

This study provides measurement data of hand bone parameters of 101 patients with TS from a single center and proposes four parameters that have implications for diagnosing TS. These results suggest that doctors should not only determine bone age, but also focus on areas of possible skeletal abnormalities when viewing hand X-rays. We also developed a deep neural network that can reliably and rapidly identify patients with TS. The clinical data used were only hand X-rays, which are beneficial for inexperienced doctors and poor areas to identify potential patients with TS and to reduce the rates of missed and misdiagnosis.

Our study has a few limitations. First, all images were obtained from our single center and were retrospective, which may introduce certain biases. In the future, we will conduct prospective validation of the model in a multicenter cohort and optimize the model based on the validation results. Second, the age of the enrolled patients was concentrated between 4 and 13 years, making it difficult to determine whether the current model is suitable for younger children, which is important for decreasing the diagnostic age. At the same time, we can conduct longitudinal follow-up of enrolled participants to analyze the changes in hand bone characteristics of TS patients with age. In future research, it will be necessary to use a large number of hand X-ray images from different age groups for analysis to optimize the model and achieve a more convincing objective result. By this method, we can also obtain data from patients with various types of chromosomal karyotypes. Although deep learning models can achieve higher accuracy, they remain a black box at present, and further research is required on the relationship between the image features of hand X-rays and diseases. At the same time, we acknowledge the limitations of building the model solely based on hand X-rays. In the future, we could adopt a multimodal approach, incorporating blood markers and facial photographs, to build the model, believing that it would yield more accurate results. However, currently using hand X-rays as the input information has strong clinical applicability and is easy to promote. Using deep learning, we can determine whether hidden and undiscovered features are strongly correlated with diseases. Finally, the model tended to use hand X-rays to identify potential patients with TS, particularly girls with short stature. However, this method

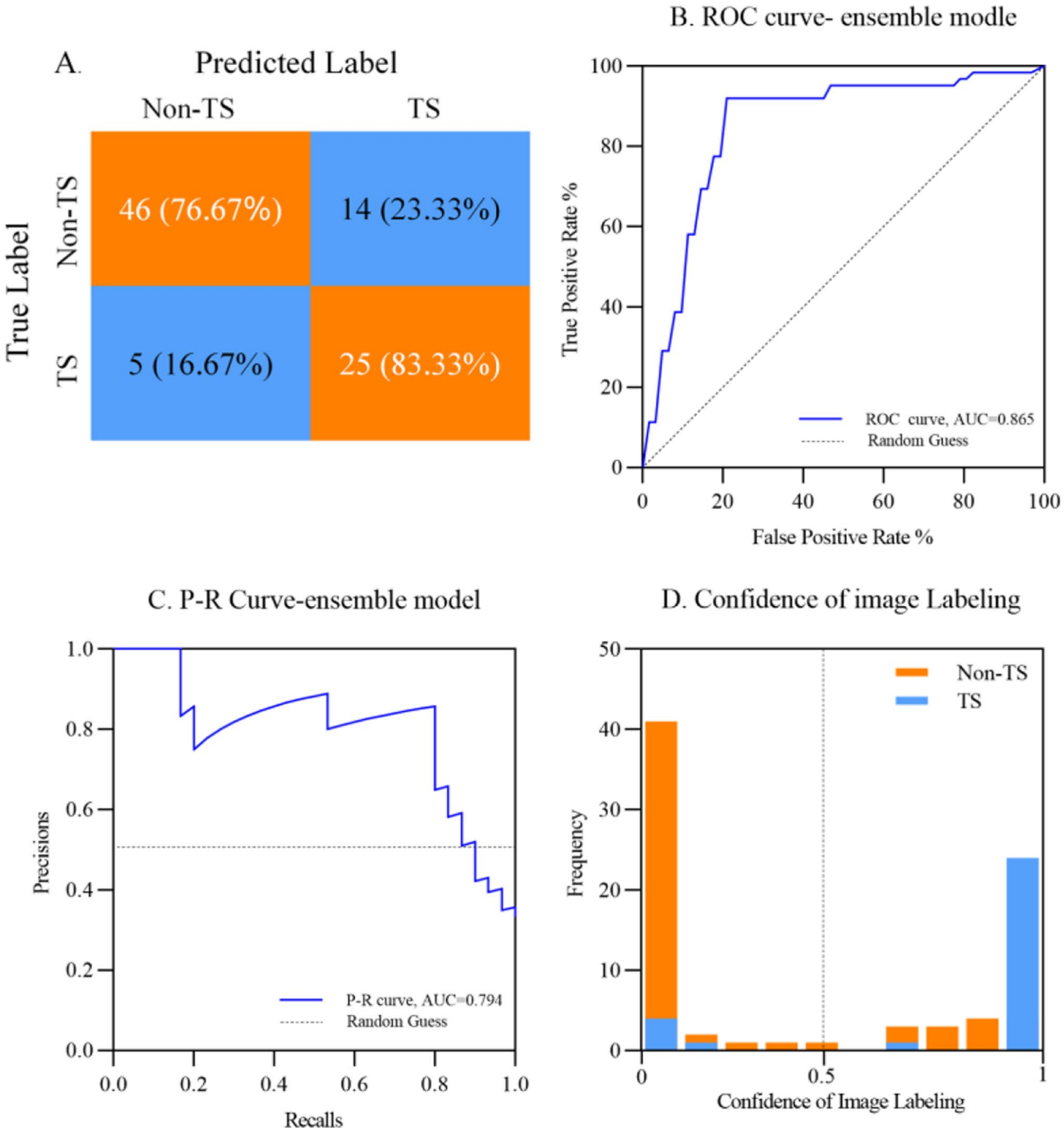

Fig. 6 Performance of the model. **A**. Confusion matrix of the classification. True positive rate (TPR) at the bottom right corner, True negative rate (TNR) at the top left corner, false positive rate (FPR) at the top right corner, and false negative rate (FNR) at the bottom left corner. **B**. ROC curve. The curve shows the relation between TPR and FPR as the threshold of the separation between positive and negative classification is varied. **C**. Precision-recall curve. Shows the relation between precision and recall. **D**. Classification score histogram. Every image is scored on a scale between 0 and 1 with threshold of 0.5, seen as a dashed line, such that all images with a higher score will be classified as positive for TS and images below as negative

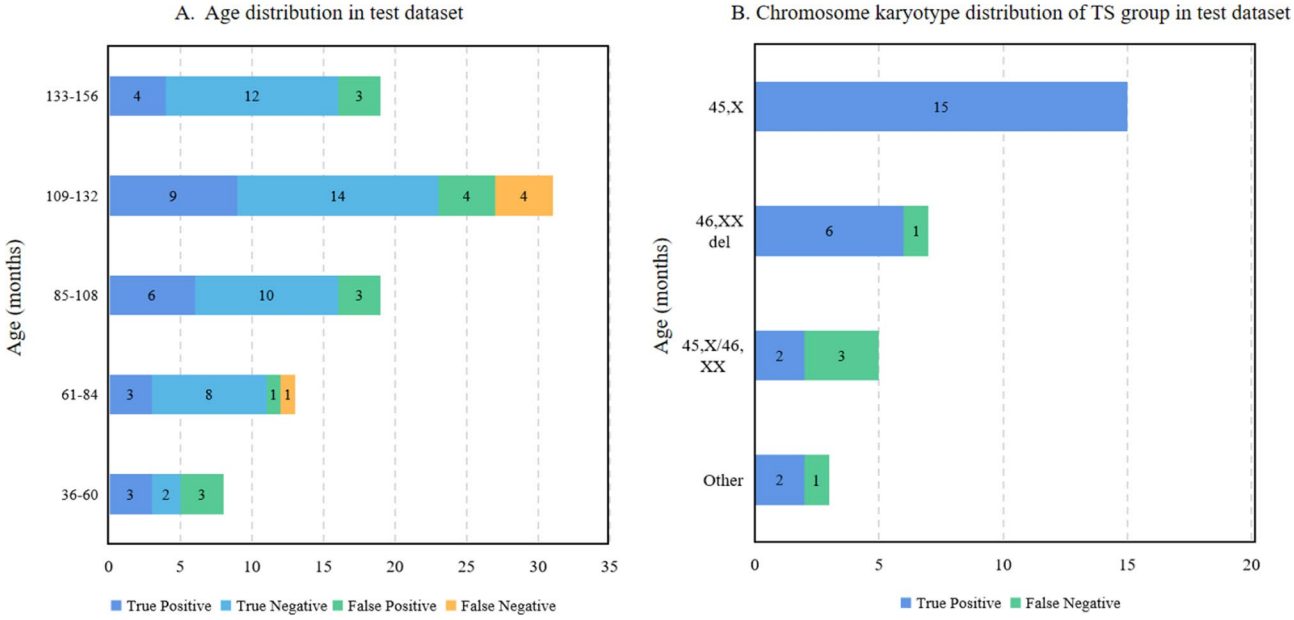

Fig. 7 Analysis of the causes of errors in test dataset prediction results. **A**. Age distribution of TR, TN, FP and FN. **B**. Distribution of chromosome karyotypes with TP and FN in the TS group

cannot directly provide a final diagnosis, which depends on further genetic testing.

Conclusion

The hand bone parameters of patients with TS differed from those of girls with normal karyotype. The signs on hand X-ray films have suggestive significance for the diagnosis of Turner syndrome, and the main parameters include the length ratio of metacarpal IV to metacarpal III, distance between ulnoradial tangents, carpal angle, and ulnar-radial angle. The image recognition model based on deep learning can effectively distinguish the hand X-rays of patients with TS and controls, and may serve as an accurate and fast way to screen for TS.

Acknowledgements
We thank the patient and his family members for their support and participation.

Author contributions
Conceptualization: WYR, WXM, LSJ. Data curation: HFH, DY, GC. Formal analysis: WYM, CY ZLQ, HYB,. Funding acquisition: WXM. Investigation: WYR, HFH, DY. Methodology: WYM, WYR. Project administration: WXM, DY. Resources: WYR, WYM, HFH. Software: WYM. Supervision: WXM, DY. Validation: WYM, HYB. Visualization: WYR, WYM. Writing—original draft: WYR, WYM. Writing—review & editing: all authors.

Funding
This work was supported by National Key R&D Program of China (2023YFC2706305) and Shanghai Clinical Medical Research Center for Children's Rare Diseases (20MC1920400).

Data availability
All data analyzed during this study are included in this article. Further inquiries can be directed to the corresponding author.

Declarations

Human ethics and consent to participate
Informed consent was obtained from the children and their parents. The biomedical research section of this study strictly adheres to ethical principles of fairness, impartiality, and non-harm, and complies with regulatory requirements such as the Helsinki Declaration and the International Code of Ethics for Research Involving Human Health. The study was approved by the Institutional Review Board of the Shanghai Children's Medical Center (No. SCMCIRB-YSWJW2023008).

Competing interests
The authors declare no competing interests.

Received: 30 June 2024 / Accepted: 24 February 2025
Published online: 08 March 2025

References

1. Gravholt CH, et al. Turner syndrome: mechanisms and management. Nat Rev Endocrinol. 2019;15(10):601–14.
2. Necic S, Grant DB. Diagnostic value of hand X-rays in Turner's syndrome. Acta Paediatr Scand. 1978;67(3):309–12.
3. Stochholm K, et al. Prevalence, incidence, diagnostic delay, and mortality in Turner syndrome. J Clin Endocrinol Metab. 2006;91(10):3897–902.
4. Swauger S, et al. Age at and indication for diagnosis of Turner syndrome in the pediatric population. Am J Med Genet A. 2021;185(11):3411–7.
5. Berglund A, et al. Changes in the cohort composition of Turner syndrome and severe non-diagnosis of Klinefelter, 47,XXX and 47,XYY syndrome: a nationwide cohort study. Orphanet J Rare Dis. 2019;14(1):16.
6. Gravholt CH, et al. Clinical practice guidelines for the care of girls and women with Turner syndrome: proceedings from the 2016 Cincinnati international Turner syndrome meeting. Eur J Endocrinol. 2017;177(3):G1–70.
7. Lee MC, Conway GS. Turner's syndrome: challenges of late diagnosis. Lancet Diabetes Endocrinol. 2014;2(4):333–8.
8. Noordman ID, et al. Karyotype - Phenotype associations in patients with Turner syndrome. Pediatr Endocrinol Rev. 2019;16(4):431–40.
9. Major J, Pusztai P, Igaz P. A short ring finger points to a diagnosis of Turner syndrome again. Lancet. 2020;395(10227):e51.
10. Nattrass GR, et al. An alternative method for determination of the carpal height ratio. J Bone Joint Surg Am. 1994;76(1):88–94.

11. Asfuroglu ZM, et al. Order of importance of anatomical risk factors in Kienbock's disease: an artificial neural network study. Hand Surg Rehabil. 2022;41(3):328–33.
12. Park E. Radiological anthropometry of the hand in Turner's syndrome. Am J Phys Anthropol. 1977;46(3):463–70.
13. He K, Z. X., Ren S et al. S., Deep residual learning for image recognition[C]// Proceedings of the IEEE conference on computer vision and pattern recognition. 2016: 770–778.
14. Tauber M, et al. Wrist anomalies in Turner syndrome compared with Leri-Weill dyschondrosteosis: a new feature in Turner syndrome. Eur J Pediatr. 2004;163(8):475–81.
15. Archibald RM, Finby N, De Vito F. Endocrine significance of short metacarpals. J Clin Endocrinol Metab. 1959;19:1312–22.
16. Kosowicz J. The carpal sign in gonadal dysgenesis. J Clin Endocrinol Metab. 1962;22:949–52.
17. Schwartz RP, Sumner TE. Madelung's deformity as a presenting sign of Turner's syndrome. J Pediatr. 2000;136(4):563.
18. Panayides AS, et al. AI in medical imaging informatics: current challenges and future directions. IEEE J Biomed Health Inf. 2020;24(7):1837–57.
19. Qiu J, et al. Large AI models in health informatics: applications, challenges, and the future. IEEE J Biomed Health Inf. 2023;27(12):6074–87.
20. Zhao Q, Yao G, Akhtar F, et al. Methods IEEE Access. 2020;PP(99):1–1. https://doi.org/10.1109/ACCESS.2020.3039867. An Automated Approach to Diagnose Turner Syndrome Using Ensemble Learning.
21. Liu L, Sun J, Li J et al. Automatic Classification of Turner Syndrome Using Unsupervised Feature Learning[C]//2020 IEEE International Conference on Systems, Man, and Cybernetics (SMC).IEEE, 2020.https://doi.org/10.1109/SMC42975.2020.9283194
22. Li J, Liu L, Sun J et al. Diagnosis and knowledge discovery of Turner syndrome based on facial images using machine learning Methods. IEEE access, 2020, 8:214866–81.https://doi.org/10.1109/ACCESS.2020.3038231
23. Hou L, Samaras D, Kurc TM et al. Patch-Based Convolutional Neural Network for Whole Slide Tissue Image Classification[C]//Computer Vision & Pattern Recognition.IEEE, 2016.https://doi.org/10.1109/CVPR.2016.266

Publisher's note